The 19th Conference of Mechanical Engineering Network of Thailand
19-21 October 2005, Phuket, Thailand

Optimization of Process Parameters in Sheet Metal Forming Using FEM

Maitri Kamonrattanapisut[1] and Surangsee Dechjarern[1]
Production Engineering Department
King MongKut's Institute of Technology North Bangkok
Bangsue, Bangkok, Thailand
Tel: 0-29132500, Fax: 0-25870029,
Email: surang@kmitnb.ac.th[1]

Abstract

In sheet metal forming process, the phenomenon of spring back and splitting are the major dimension accuracy problems. These two phenomenon are influenced by a combination of various process parameters, such as the tool geometry, friction contact condition and material properties. At the present time, design of sheet metal forming die geometry is primarily based on trial and error. The experience of the die designer, the press operator and the die corrector to a large extent determine the performance of the process. This work aims at the numerical investigation on spring-back and splitting characteristics of the major process parameters of sheet metal forming. A three dimensional elastoplastic finite element analysis of a forming process of AMS 5504 stainless steel has been successfully developed. The material flow stress used in this work was obtained from the viscous pressure bulge test under biaxial state of stress. The model was validated with the experimental tests and the results agree well. The effective strain and percentage in thinning distributions were examined. The effective strain exhibit the considerable thickness-wise variation, particularly in the material region near the punch corner. Sensitivities analysis done based on forming limit curve (FLC) demonstrates that magnitude of global splitting are influenced by the process parameters i.e. the die entry radius, punch-die clearances and the blank holder force. The optimization process was carried out and the convergence was reached after 22 iterations.

Keywords: 3-5 words, 10 point size

1.Introduction

Sheet metal forming is widely used within automotive industries to produce finished products without any expensive finishing operations. In sheet metal forming, high forming quality demands that any kind of rupture or wrinkling should be avoided. The rupture or wrinkling are influenced by a combination of various process parameters, such as the tool geometry, friction contact condition and material properties. At the present time, design of sheet metal forming tool geometry is primarily based on trial and error and the experience of the die designer. As progress of simulation technologies and upgrades of computer features, numerical simulation of sheet metal forming processes has become a very powerful tool in the automotive industry. Recent progress makes it possible to obtain accurate and reliable results from simulation [1,2,3]. The aim of the present work is the determination of the optimum process parameters, such as blank holder forces and optimal die radius to reduce the risk of rupture by the use of the forming limit diagram (FLD) [4,5].

2. Finite element model of sheet metal forming

2.1 Geometry and Boundary Conditions

The initial geometry and dimension of the 3D finite element model of a metal forming process is shown in Figure 1. The summaries of process parameter used are shown in Table 1. The worksheet, the punch, the die and the blank holder were initially modeled with 500, 1,200, 1,500 and 1,500 elements and the adaptive remeshing scheme was implemented to optimize between the computational time and accurate prediction. In this model, the punch was constrained in all directions. The die was subjected to move in Y direction at a constant speed and constrained against movements in X and Z directions. The binder was pressed down with five different holder forces. The worksheet is free to moved in any direction.

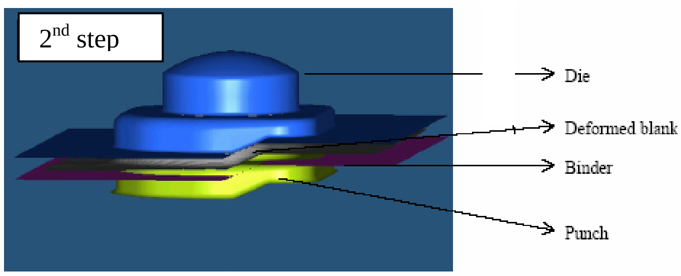

Figure 1: Finite element model of the sheet metal forming process

Table 1: Simulation conditions of the Sheet metal forming

Conditions	
Workpiece material	AMS 5504
Initial sheet thickness	1.6 mm
Initail sheet size	280 * 300 mm
Clearance (x thickness)	1, 1.1, 1.2
Blank holder force	200, 230,250,280,300
Forming speed	1000,2000,3000,4000,5000

2.2 Material Property

The workpiece material was assumed to be an isotropic elasto-viscoplastic using Krupkowski-Swift law,

$$\sigma(\varepsilon) = k\,(\varepsilon_0 + \varepsilon)^n \quad (1)$$

where ε_0= offset strain, ε= Effective strain, **k**= Hardening coefficient ,**n** = Hardening Exponent. The anisotropy effect in sheet forming can be considered by the ratio of the plastic deformation (the Lankford value) *R,* which can be found as

$$R = \frac{\epsilon_w}{\epsilon_t} = \frac{\ln(w_f/w_o)}{\ln(t_f/t_o)}, \quad (2)$$

where w_f means the final width, w_0 the original width, t_f the final thickness, and t_0 the original thickness. The measured values for each of the directions *R0, R45,* and *R90* to the rolling direction are provided in table 2. Previous works [1,2], the deformation properties of sheet material were normally determined using a standard tensile test under uniaxial deformation conditions. During sheet metal forming operations the material deforms under biaxial conditions. Under the biaxial tensile this state of stress, the true strain level may reach a higher magnitude than that of the standard tensile test. This may cause significant errors in process simulations. In this work, material properties obtained from the viscous pressure bulge test (VPB) under biaxial state of stress were used [6]. Material properties used for all components are summarized in Table 2. Coulomb friction contact conditions were applied to the interface between the punch and sheet, sheet and blank holder, holder and die and die and sheet. The friction coefficient of 0.15 was used for all contacts.

Table 2: Mechanical property of AMS 5504 [6]

Mechanical property	
Tensile strength	348.915 (Mpa)
Modulas' young	210e+03 (Mpa)
Yield stress	216 (Mpa)
Poisson's Ratio	0.3
Hardening Exponent	0.21
Hardening coefficient	597.390
Offset strain	7.874e-03
Anisotropy coeffcients	
*R*0=1.14, *R*45=0.94, *R*90=1.43	

3. Results

3.1 Validation of Finite Element Analysis

Figure 2a and 2b shows the experimental part after piecing and the simulation result respectively. Lengths were measured on three sides of the parts so that the results can be used to validate the finite element prediction. It can be seen from Figure 2c that the FEM results are in good agreement with the experiments. The predictions are only 5% higher than the experimental results. This could be due to the slight inaccurate friction coefficient and the material anisotropy.

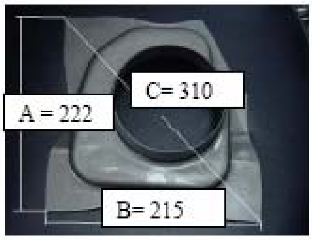

(a)

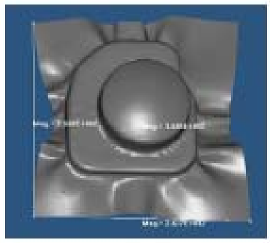

(b)

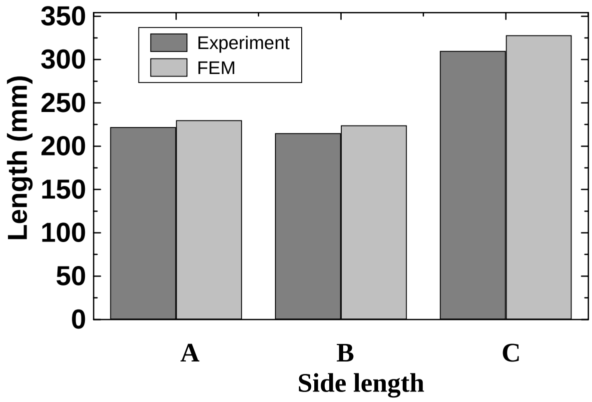

(c)

Figure 2: (a) Experimental part (after piecing), (b) finite element result and (c) the comparison between the predicted and experimental lengths

3.2 The Deformed Shape and strain distribution

The FLD is the set of strains obtained on each element by the numerical simulation during the process. The forming limit diagram (FLD) of the deformed part predicted by FEM and the experimental part are shown in Figure 3a and 3b respectively. The forming limit diagram is commonly used for identifying the forming failure. The forming limit curve (FLC) given by experiments or numerical prediction of ($\varepsilon 2$, $\varepsilon 1$) value for each material, limits the safe region within FLD. Failure occurs during deep drawing at a material point, if the principal strains ($\varepsilon 2$, $\varepsilon 1$) for this point is above the FLC. In this work, the FLC line is the red line. Wrinkle is likely to occur when the minimum principal strains are much larger than the maximum one. The blue line in Figure 3a presents this wrinkle line.

It is clear from Figure 3 that rapture (red area) takes place around the corner of top curve and wrinkle (blue area) arises for both the finite element and the experiment results. The finite element model correctly predicted the rapture and wrinkle.

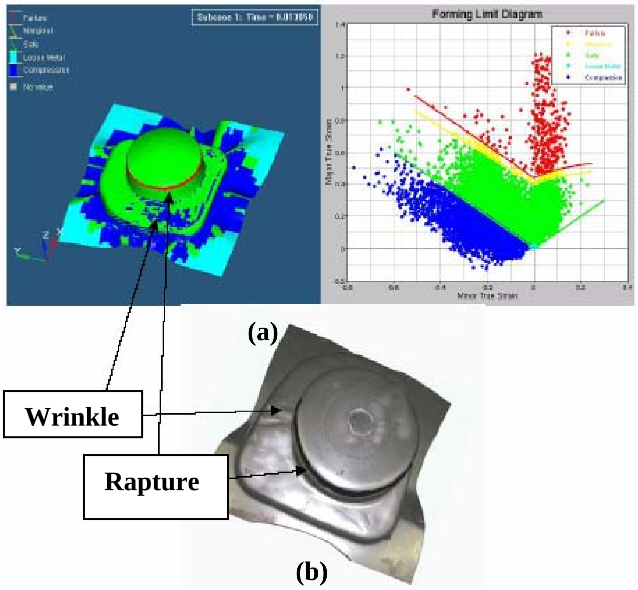

Figure 3: a) Forming limit diagram of part showing rapture prediction, b) Real part without rapture

The distribution of thinning is shown in Figure 4. The result shows the localized excessive thinning around the corner of the top curve causing rapture. The region where wrinkle transpires exhibits low percentage of thinning or even increases in thickness. Figure 5 shows the distribution of the effective strain distributions. The effective strain exhibit the considerable thickness-wise variation, particularly in the material region near the top corner. The effective strain accumulated and reached the maximum value at the end of the forming process of around 0.8. This is when the material starts to yield and cracks form. The effective strain distribution at the wrinkle area is only 0.05. This shows that the material around that area does not deform and this causes wrinkle.

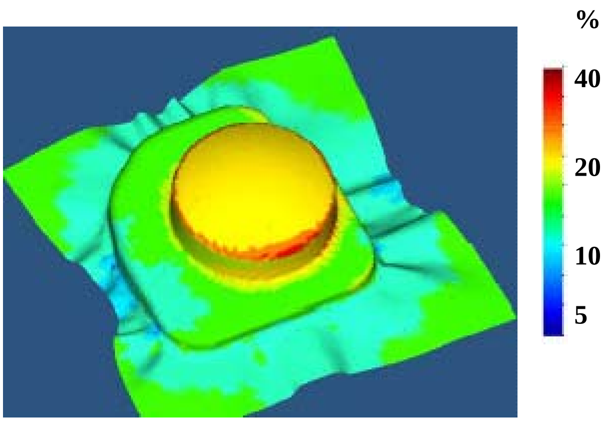

Figure 4: The distribution of thinning (in percentage)

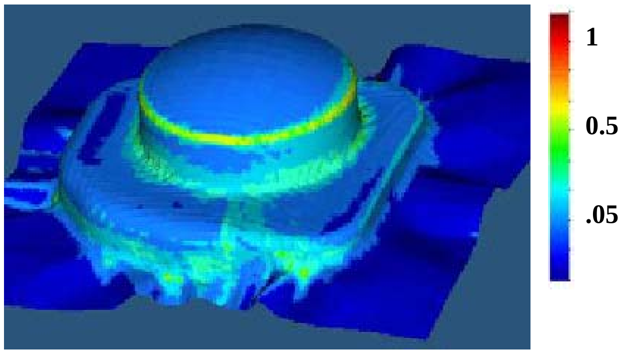

Figure 5: The distribution of effective strain

4. Sensitivity analysis

The evaluation criterion for forming failures is identified as rupture criterion and wrinkling criterion. Both criterions are included in the objective function. In order to perform an analytical evaluation of the sensitivities, the objective function is expressed in terms of the distances from the "*secure FLC*" (see Figure 6) but only for the elements where the major strain ε_1 is greater than $\psi(\varepsilon_2)$. A "*secure FLC*" function $\psi(\varepsilon_2)$ is defined as:

$$\psi(\varepsilon_2) = \varphi(\varepsilon_2) - s \tag{3}$$

where s is a "*safety*" margin from the FLC. Therefore, the global objective function is the sum of all the element objective function, J^e, which is given by:

$$\begin{cases} J^e = (\varepsilon_1^e - \psi(\varepsilon_2^e))^{2p} & \text{if } \varepsilon_1^e > \psi(\varepsilon_2^e) \\ J^e = 0 & \text{if } \varepsilon_1^e \le \psi(\varepsilon_2^e) \end{cases} \tag{4}$$

where p equal to 2. Four parameters were investigated in the sensitivity analysis, i.e. die entry radius, blank holder forces, punch-die clearances and forming speeds.

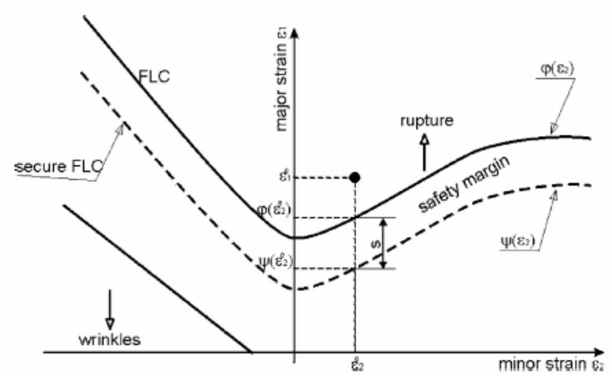

Figure 6: The definition of the objective function based on FLC [5]

4.1 Influence of blank holder force on FLC

In the simulations, the values of the die entry radius, punch-die clearance and the forming speed are kept constant at 3 mm, 1.1t and 3000 mm/s respectively. It is clear from Figure 7 that the normalized objective function is influenced by the holder force. The objective function is nearly stable for the holder force of 200-250 kN. At the holder force of 270 kN, the objective function is peaked at around 1.2. It means that the deformed FEM part has the highest amount of damage and more cracks. The objective function is then declined.

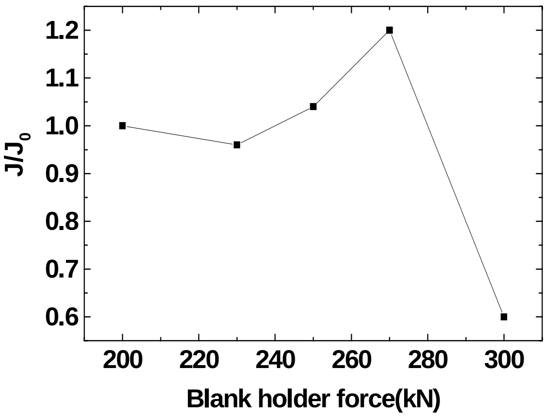

Figure 7: The influence of the blank holder force on objective function, J/J_0.

4.2 Influence of punch-die clearance on FLC

During this study, the values of the values of the die entry radius, blank holder force and the forming speed are kept constant at 3 mm, 220 kN and 3000 mm/s respectively. Figure 8 shows that the objective function decreases with the punch-die clearance until the clearance reaches the value of 1.1t, where the lowest value of the objective function is 0.8. After this value, the objective function increases again.

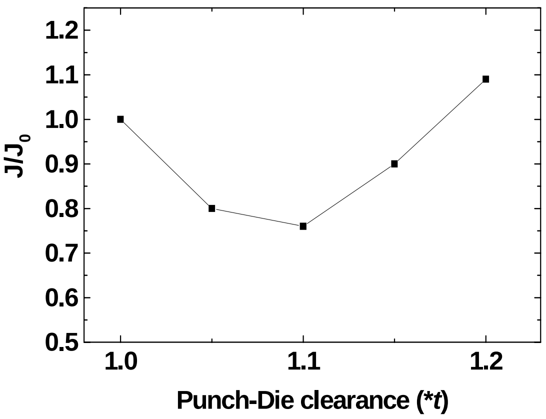

Figure 8: The influence of the punch-die clearance on objective function, J/J_0.

4.3 Influence of die entry radius on FLC

In the simulations, the values of the blank holder force, punch-die clearance and the forming speed are kept constant at 230 kN, 1.1t and 3000 mm/s respectively. Figure 9 shows that the normalized objective function decreases as the value of the die entry radius increase. The lowest value of the objective function is 0.3 and it is the lowest of any other case studies. It is clear that the die entry radius influenced the possibility of rapture more than any other parameters studied here. This could be the reason for the extensive industrial use in alternating this parameters to reduce the riskof rapture. After the die entry radius of 5 mm, the objective function seem to be stable.

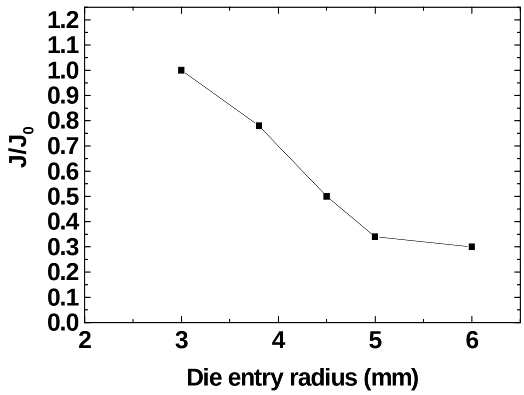

Figure 9: The influence of the die entry radius on objective function, J/J_0.

4.4 Influence of forming speed on FLC

During this study, the values of the values of the die entry radius, blank holder force and the blank holder force are kept constant at 3 mm, 220 kN and 270 kN respectively. Figure 9 shows that the variation of the amount of normalized objective function value and forming speed. The objective function value is seemed to be stable with the increase of workpiece thickness. However, the effect of the forming speed on the rapture and wrinkle (objective function) is not as significant as that of the die entry radius and punch/die clearance.

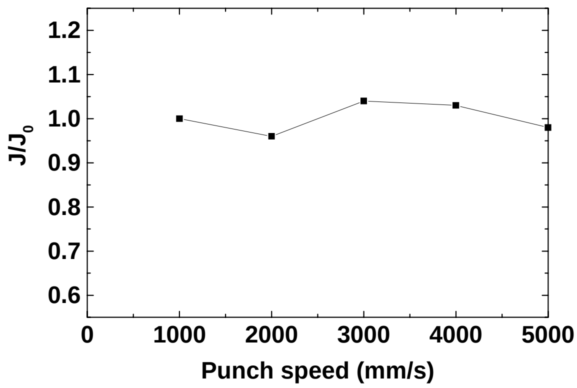

Figure 10: The influence of the punch speed on objective function, J/J_0.

5. Parameter Opimization

Mathematical modeling is an important component involved in the optimization process. The model contains three components: design variable, objective function and constraints. A typical formulation can be written as

min $f(x)$

subject to $g_i(x) \leq 0 \; (i = 1, 2, \ldots, m)$ (1)

where x is the design variable, g_i the inequality constraint and $f(x)$ is the objective function.

5.1 Optimization parameter setting

Sensitivity analysis results indicated that the important influences of the blank holder force, punch-die clearance and the die entry radius on the reducing the risk of rapture. Thus, the design variables of this problem were the die entry radius, D; the punch-die clearance, C, and the blank holder force, F_b. The maximum die entry radius (D) is restricted by the fitting of this part into the final part geometry. The size of the press and the economic of the press energy limit the amount of the blank holder force, F_b. The values of the design variable were 6 mm $\geq D \geq$ 3 mm; $1.2t \geq C \geq 0.8t$ (t = the sheet thickness), and 200 kN $\geq F_b \geq$ 300 kN. The optimization goal is to find the minimal value of the global objective function, thus the sum of the element objective function (Eq. 4).

The maximum percentage of thinning was used as a constraint to avoid localized defects within the deformed sheet when using this objective function. The maximum value of the thinning strain should be less than 25%.

5.2 Optimization methodology

Solution to optimization problem involves the determination of the search direction and magnitude of change in design variables along the search direction. The search direction for this problem was evaluated using conjugate gradient method. The gradients of the objective function and the constraints required to evaluate the search direction are obtained by the forward difference method [8]. The golden section method [8] was used for the one-dimensional search to find the magnitude of change in the design variable (α) along the search direction. Constraints on the design variables were used in finding the initial limits for finding α along the search direction. the optimization procedures are stated as follows:

(a) Determine a search range of the design variable α in which the optimal solution may exist.
(b) Select two trial values of the design variable α, simulate the whole forging processes, respectively, and finally get two solutions of the objective functions.
(c) After comparing two solutions of objective functions, decrease the search range again.
(d) Select a new trial value of the design variable and simulate the whole forging process again. Finally, get a new objective function solution.
(e) Decrease the search range again after comparing the solutions of the objective functions.
(f) Repeat above steps until the range of the design variable is sufficiently small. Then the optimal design variable is obtained.

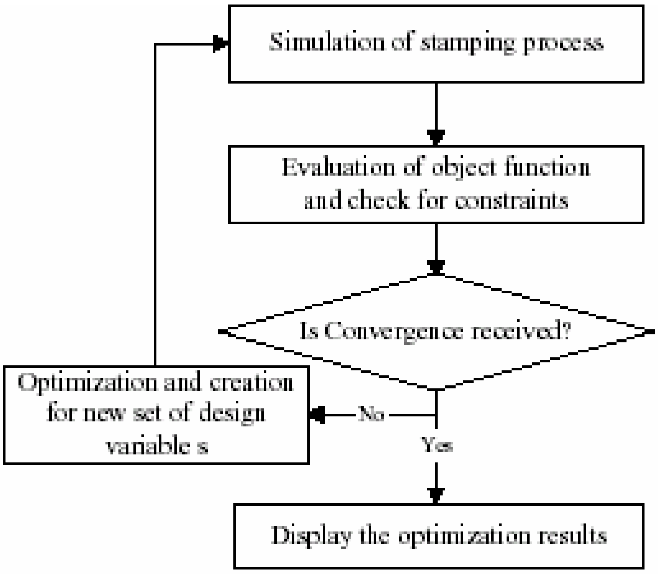

Figure 11: Optimization procedure

5.3 Optimization results

Figure 12 shows the evolution of the objective function during the optimization. It is clear that convergence was achieved after 32 iterations. The value of design function decrease by 80 %. Figure 13 shows the decrease of the percentage of thinning strain from more than 80% down to under 25 % during optimization. This indicates more uniform thickness distribution within the deformed part after the optimization process. Figure 14 shows the evolution of the design variable (die entry radius) during the optimization. It can be seen that the value of the die entry radius was stabled at the beginning of the optimization process and then increase slowly after 9 iterations. The value of the die entry radius then fluctuated between 5 – 6 mm and reached the optimum point at the value of 5.2 mm.

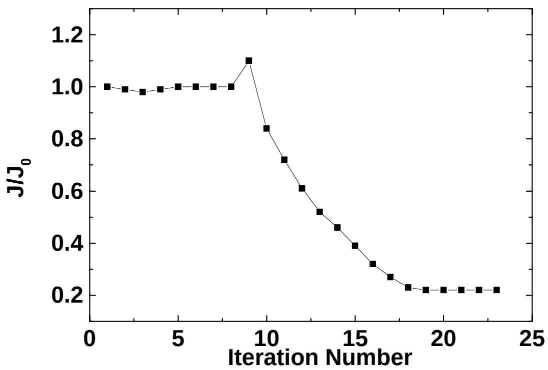

Figure 12: The variation of the global objective function with the number of optimization iteration

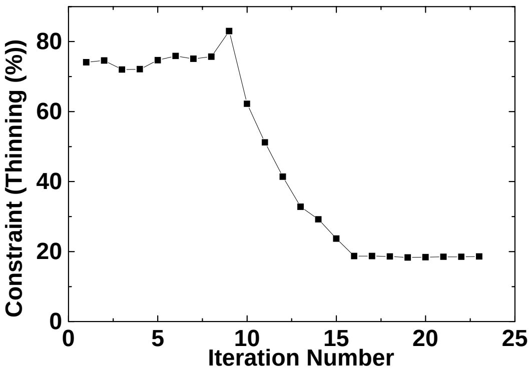

Figure 13: The variation of the constraint (% thinning) with the number of optimization iteration

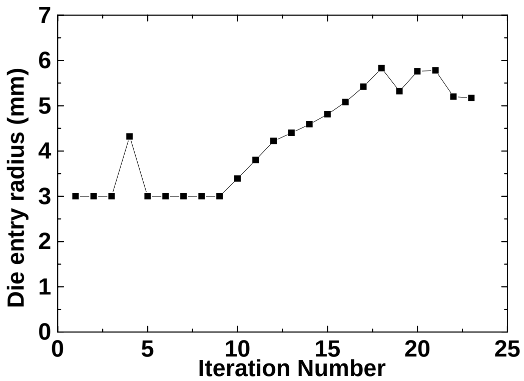

Figure 14: The variation of the design variable (die entry radius) with the number of optimization iteration

Figure 15 shows the evolution of another design variable (the punch-die clearance) with the number of iteration during the optimization. It can be seen that values of the punch-die clearances fluctuated only slightly around the value of 1.2 time thickness (t). It then started to decrease rapidly at the iteration number 10 and reached its lowest value of 0.8t at the iteration number 14. The punch-die radius increases again in value and fluctuated heavily before its reach the optimum condition at the value of 1.07t. The optimum value of the blank holder force is 235 kN.

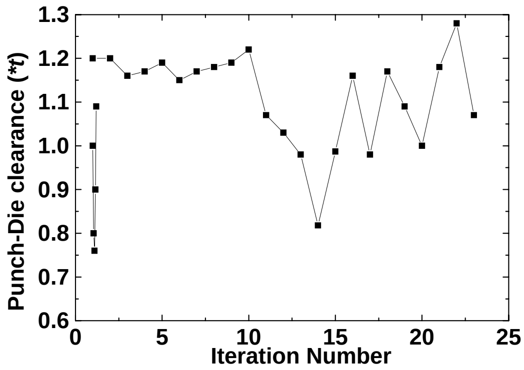

Figure 15: The variation of the the punch-die clearance with the number of optimization iteration

Figure 16 shows the forming limit diagram of the part using optimized FEM parameters. It is clear that there is no rapture occurs within the optimized deformed part. The optimum parameters were introduced into the real die and the sheet metal forming was carried out. The final experimental part was then compared with the FEM results as shown in Figure 16. The results are successfully compared with those on the process used by production.

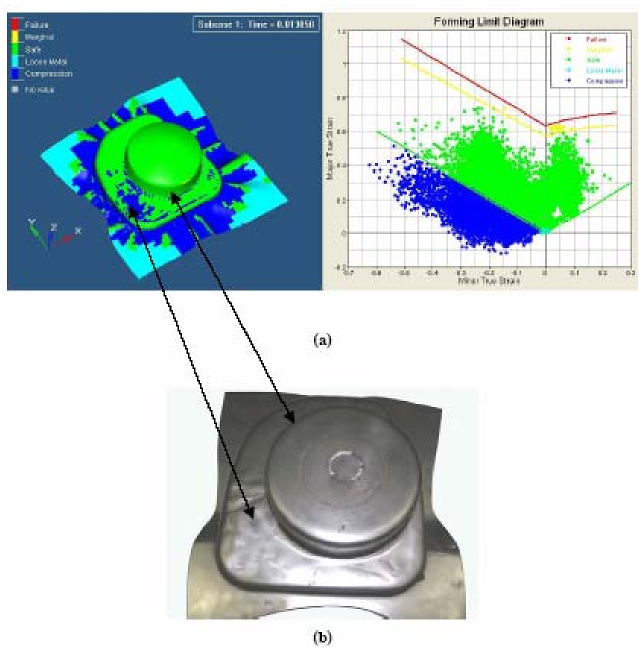

Figure 16: a) Forming Limit Diagram of part after optimization b) Real part without rapture

6. Conclusions

The isotropic elastro-plastic finite element model of sheet metal forming process was successfully developed using the data obtained from the viscous pressure bulge test under biaxial state of stress. The model was validated using the experimental results. The FEM prediction of the size of the deform shape are within 5% of the experimental results. This could be because of the inaccurate value of friction coefficient. The effective strain and percentage in thinning distributions were examined. The effective strain exhibit the considerable thickness-wise variation, particularly in the material region near the punch corner. Sensitivities analysis was carried out based on forming limit diagram (FLD) demonstrate that magnitude of global splitting are influenced by the process parameters i.e. the die entry radius, punch-die clearances and the blank holder force. The forming speed was found not to influence the splitting of deformed part. The optimization process was carried out and the convergence was reached after 22 iterations. The final value of the normalized objective function and constraint were 0.2 and less than 25% respectively. The optimum design variables are the punch-die clearance of 1.07 time of the sheet thickness, the blank holder force of 235 kN and the die entry radius of 5.2 mm. The optimum parameters were introduced into the real die and the sheet metal forming was carried out. The final experimental part was successfully free of splitting.

Acknowledgments

The financial support by the Thailand Automotive Institute and Brother Auto part LTD are highly appreciated.

References

[1] T. Ohata, Y. Nakamura, T. Katayama, et al., Development of optimum process design system by numerical simulation, J. Mater. Proc. Technol. 60 (1996) 543–548. optimization methods, in: Proceedings of the Numiform'98, 1998, pp. 787–792.
[2] Hariharasudhan Palaniswamy, Gracious Ngaile, Taylan Altan. Opimization of blank dimensions to reduce springback in the flexforming process. J. Mater. Process. Technology. 105 Volume146 (2004).
[3] C. Knopf-Lenoir, H. Naceur, J.L. Batoz, Y.Q. Guo, Modeling and optimum design of drawbeads in sheet metal forming, in: M. Geiger (Ed.), Advanced Technology of Plasticity, vol. III, Proceedings of the Sixth International Conference on Technology of Plasticity, Nuremberg, September 19–24, 1999, pp. 2055–2060.
[4] Xiaoxiang Shi a,., Jun Chenb, Yinghong Peng b, Xueyu Ruan, A new approach of die shape optimization for sheet metal forming processes, Journal of Materials Processing Technology (2004)
[5] H. Naceur., A. Delaméziere, J.L. Batoz , Y.Q. Guob, C. Knopf-Lenoir, Some improvements on the optimum process design in deep drawing using the inverse approach, Journal of Materials Processing Technology 146 (2004) 250–262.
[6] Gerhard Gutscher, Hsien-Chin wu, Gracious Ngail, Taylan Altan. Determination of flow stress for sheet metal forming using the viscous Pressure bulge (VPB) test, Journal of Mater. Process. Technology. 105, Volume146 (2004).
[7] J.S. Arora, Introduction to Optimum Design, McGraw-Hill, New York, 1989
[8] Myers, R. H., and Montgomery, D. C., *Response Surface Methodology: Process and Product Optimization Using Designed Experiments*, John Wiley and Sons, 1995.
[9] HyperWork User's Manual, Version 6.0, Altair Engineering, Inc., Troy, MI 48084, 2003.